Title
MR and CT Imaging for the Evaluation of Pulmonary Hypertension

Journal
JACC Cardiovascular Imaging, 9(6)

ISSN
1936-878X

Authors
Freed, Benjamin H
Collins, Jeremy D
François, Christopher J
et al.

Publication Date
2016-06-01

DOI
10.1016/j.jcmg.2015.12.015

Peer reviewed

HHS Public Access

Author manuscript

JACC Cardiovasc Imaging. Author manuscript; available in PMC 2017 June 01.

Published in final edited form as:

JACC Cardiovasc Imaging. 2016 June ; 9(6): 715–732. doi:10.1016/j.jcmg.2015.12.015.

Magnetic Resonance and Computed Tomography Imaging for the Evaluation of Pulmonary Hypertension

Benjamin H. Freed, MD[1], **Jeremy D. Collins, MD**[2], **Christopher J. François, MD**[3], **Alex J. Barker, PhD**[2], **Michael J. Cuttica, MD**[3], **Naomi C. Chesler, PhD**[4], **Michael Markl, PhD**[2], and **Sanjiv J. Shah, MD**[1,5]

[1]Division of Cardiology, Department of Medicine, Northwestern University Feinberg School of Medicine, Chicago, IL

[2]Department of Radiology, Northwestern University Feinberg School of Medicine, Chicago, IL

[3]Department of Radiology, University of Wisconsin, Madison, WI

[4]Division of Pulmonary and Critical Care Medicine, Department of Medicine, Northwestern University Feinberg School of Medicine, Chicago, IL

[5]Feinberg Cardiovascular Research Institute, Northwestern University Feinberg School of Medicine, Chicago, IL

Abstract

Imaging plays a central role in the diagnosis and management of all forms of pulmonary hypertension (PH). While Doppler echocardiography is essential for the evaluation of PH, its ability to optimally evaluate the right ventricle (RV) and pulmonary vasculature is limited by its 2D planar capabilities. Magnetic resonance imaging (MRI) and computed tomography (CT) are capable of determining the etiology and pathophysiology of PH, and can be very useful in the management of these patients. Exciting new techniques such as RV tissue characterization with T1 mapping, 4D flow of the RV and pulmonary arteries, and CT lung perfusion imaging are paving the way for a new era of imaging in PH. These imaging modalities complement echocardiography and invasive hemodynamic testing, and may be useful as surrogate endpoints for early-phase PH clinical trials. Here we discuss the role of MRI and CT in the diagnosis and management of PH, including current uses and novel research applications, and we discuss the role of value-based imaging in PH.

Address correspondence to: Sanjiv J. Shah, MD, FACC Associate Professor of Medicine, Division of Cardiology, Department of Medicine, Feinberg Cardiovascular Research Institute, Northwestern University Feinberg School of Medicine, 676 N. St. Clair St., Suite 600, Chicago, IL 60611 Phone: 312-695-0993, Fax: 312-253-4470, *sanjiv.shah@northwestern.edu*.

CONFLICT OF INTEREST DISCLOSURES: None.

Keywords

pulmonary hypertension; magnetic resonance imaging; computed tomography; right ventricle; pulmonary vasculature; anatomy; physiology

INTRODUCTION

Pulmonary hypertension (PH) is a common hemodynamic abnormality that reflects a variety of diseases of the heart and pulmonary vasculature (Table 1) (1,2). Imaging is critical in the diagnostic evaluation of all types of PH. Not only does it provide the first clue that pulmonary artery (PA) pressures may be elevated, but it also allows the direct visualization of the right ventricle (RV) and its adaptation (or maladaptation) to worsening pulmonary vascular function. Furthermore, imaging tests are essential for determining the etiology of PH. While two-dimensional (2D) Doppler echocardiography remains the most commonly used imaging modality for cardiac and hemodynamic evaluation in PH, its ability to comprehensively and accurately evaluate the RV and pulmonary vasculature is limited by its 2D planar capabilities. In addition, while echocardiography can assist in determining whether left heart disease or congenital heart disease is the cause of PH, several other causes of PH (e.g., lung disease, chronic thromboembolic disease, etc.) require additional imaging modalities.

Advanced imaging modalities such as magnetic resonance imaging (MRI) and computed tomography (CT) overcome the aforementioned limitations while providing an additional layer of mechanistic insight that is not possible with echocardiography alone. Examples of novel MRI and CT techniques include four-dimensional (4D) flow assessment of the PA on MRI, tissue characterization of the RV on MRI, and quantification of lung perfusion on dual-energy CT. Here we discuss the current role of MRI and CT in the diagnosis and management of PH; novel research applications of these imaging techniques; a clinical assessment of the relative utility of the various imaging modalities (including echocardiography); the role of MRI in PH clinical trials; and an assessment of value-based imaging in PH.

MAGNETIC RESONANCE IMAGING: CURRENT APPROACHES IN PULMONARY HYPERTENSION

Right ventricular size and function

The RV is a critical barometer of cardiovascular health in patients with PH. Several studies have demonstrated the prognostic significance of RV function in PH, whether evaluated indirectly using invasive hemodynamic testing (e.g., right atrial pressure, cardiac output) or directly via non-invasive imaging (e.g., RV ejection fraction) (3). Cardiac magnetic resonance (CMR) is the reference standard for the assessment of RV size and systolic function (4). Owing to the non-symmetric, pyramidal chamber configuration, quantitation of RV size and systolic function is a unique challenge even when evaluated with CMR (5). Some investigators have advocated for orienting short-axis slices parallel to the tricuspid baseline, as such an orientation is rarely in the same plane as short axis slices aligned for left

ventricular (LV) analysis (6). However, short axis oriented images pose challenges in identifying the RV base plane during systole and diastole and require cross-referencing with RV 2-chamber and RV inlet-outlet imaging to ensure accurate definition of the base plane. Other authors have advocated to contour the RV from transaxial images mitigating difficulties identifying the RV base plane (6). With this approach, Jauhiainen et al. demonstrated improved reproducibility of RV volumes compared to short axis images optimized to the RV axis (6).

Quantification of RV chamber size and systolic function requires electrocardiographically (ECG)-gated cine images. This technique often uses segmented balanced steady state free precession (bSSFP) imaging with effective temporal resolutions < 50 msec and enabling a per-slice acquisition time on the order of 5–15 seconds, depending on heart rate, spatiotemporal resolution, and parallel imaging capabilities. Patients with slower heart rates, irregular rhythms, or dyspnea limiting breath-holding are challenging to image with CMR. Real-time cine imaging permits assessment of regional wall motion, but is limited due to necessary tradeoffs in spatial and temporal resolution (7). The use of advanced imaging acceleration techniques such as compressed sensing, radial sampling trajectories, and three-dimensional (3D) approaches with ECG-gating and self-gated respiratory navigation are promising techniques to improve CMR image quality in patients with dyspnea or irregular rhythms, both of which commonly occur in patients with PH.

RV quantification during CMR yields accurate measures of RV size (RV end-diastolic and end-systolic volume), stroke volume (SV), myocardial mass, and ejection fraction (8). Maladaptive changes in CMR-derived RV end-diastolic volume, end-systolic volume, and ejection fraction—indicative of RV remodeling and dysfunction—have been associated with a worse prognosis in PH patients on optimal medical therapy (3). Similarly, a reduced SV on CMR has been linked to increased mortality, both at baseline and on follow-up imaging after initiation of therapy (9).

Interventricular septal changes

The interventricular septum (IVS) is known to play a critical role in the pathophysiology of PH (10). As PA systolic pressure (PASP) increases, RV systolic pressure exceeds that of the LV and the resulting IVS shift towards the LV impedes cardiac output (11). Mechanical asynchrony, wherein RV contraction time is prolonged compared to LV contraction time, is also thought to contribute to this process (12,13). In addition, as RV diastolic pressure increases with progressive RV failure, IVS flattening occurs during diastole thereby impeding LV filling, further reducing cardiac output. Because of its superior spatial resolution, CMR cine short-axis images provide a detailed view of this dynamic relationship between the RV and LV (14,15). Beyond simply correlating the degree of septal flattening to PASP, studies using CMR have attempted to quantify the shape and deformation of the IVS using 3D analysis in patients with PH (16). The changes to the IVS that occur throughout the cardiac cycle may, over time, be responsible for the delayed enhancement commonly found in the RV insertion points on CMR (17).

While CMR cine imaging provides excellent spatial resolution, free breathing sequences provide real-time physiologic assessment of IVS dynamics (Figure 1). These sequences are

particularly helpful in understanding the ability of the RV to handle volume overload. During inspiration, negative intrathoracic pressure creates a suction effect in the thorax, which results in increased blood flow from the systemic veins into the right heart. While some IVS flattening is expected during inspiration to accommodate the increased volume of blood, significant IVS flattening at peak inspiration is indicative of a vulnerable or dysfunctional RV.

Pulmonary vasculature function

In a number of studies, the standard phase contrast technique (2D phase contrast magnetic resonance imaging [PC-MRI], with single direction velocity encoding along the through-plane direction) has been applied to evaluate changes in blood flow in patients with pulmonary arterial hypertension (PAH). Pelc et al. initially noted that main PA flow at peak systole in PAH patients was more spatially heterogeneous and demonstrated a greater percentage of retrograde flow (18). Building on this observation, a number of researchers have quantified bulk flow hemodynamics in the PAs. Among them, Ley performed a detailed study of 25 PAH patients and 25 controls to compare the PA peak velocity, average flow, time-to-peak velocity, velocity rise gradient, and pulmonary distensibility (19). In this study, CMR values were also compared to transthoracic echocardiography and right heart catheterization. In comparison to the controls, the PAH patients showed significantly reduced pulmonary velocities ($P = 0.002$), blood flow ($P = 0.002$), and pulmonary distensibility ($P = 0.008$). The patients also showed a shorter time-to-peak velocity ($P<0.001$) with a steeper velocity rise gradient ($P=0.002$). In addition, a number of authors have observed highly heterogeneous cross-sectional area flow profiles and retrograde flow in the main PA of PAH patients (20–22).

The pulsatility of deformation of the main PA is useful as an index of PA stiffness (23). A related measure called PA relative area change can also be calculated (24); decreased values of main PA relative area change indicate increased PA stiffness and have been associated with increased mortality (25). Magnetic resonance angiography (MRA) can also provide information on pulmonary vascular function. Using data from signal intensity curves on MRA, Ohno et al. found that prolonged mean transit time and decreased pulmonary blood flow were common in patients with PAH (26,27) while Swift et al. suggested that these parameters have prognostic significance in these patients (28).

Right ventricular delayed enhancement

Delayed enhancement imaging on CMR is a well-established technique to identify focal myocardial abnormalities. RV insertion point (RVIP) enhancement, a common finding in patients with PH, appears as regions of poorly marginated mesocardial scar in the basal-to-mid chamber along the anterior and inferior RV septal insertion points (Figure 2). This pattern of delayed enhancement is strongly associated with elevated PA pressures, as well as RV dilation and hypertrophy (29), and has also been associated with adverse outcomes in patients with PH (30). RVIP enhancement at the basal anteroseptal insertion has been associated with reduced regional RV contractility suggesting a structure-function relationship (31). Lending support to structural alterations in this region, RV septomarginal trabeculations inserting into the basal-to-mid chamber anteroseptum are significantly

hypertrophied in PH subjects, correlating with elevated pulmonary pressure and vascular resistance (32). These findings suggest increased mechanical stress at the anteroseptal insertion and may explain the pattern of delayed enhancement identified.

MAGNETIC RESONANCE IMAGING: NOVEL APPROACHES IN PULMONARY HYPERTENSION

MRI approaches to the evaluation of PH are rapidly evolving. The following section includes several techniques that are still in development and likely will not be available and ready for routine clinical use for some time. However, these novel imaging approaches can provide unique insight into the pathophysiology of PH and should be examined in prospective research studies (including PH clinical trials) to determine their utility relative to conventional imaging approaches.

Right ventricular T1 mapping

While delayed enhancement imaging identifies regional myocardial abnormalities, a newer MRI technique, T1 mapping, can potentially identify diffuse myocardial abnormalities by either measuring native RV T1 time without the need for contrast or extracellular volume fraction based on pre- and post-contrast T1 times (33). Both metrics can be considered surrogate markers for ventricular fibrosis (34,35). A recent paper showed a strong correlation between T1 mapping values of the RV insertion points and indices of RV dysfunction (36). However, a better use of this technique may be the detection of diffuse interstitial abnormalities in the RV (37).

Kawel-Boehm et al. tested the feasibility of RV T1 mapping using standard modified look-locker inversion (MOLLI) recovery in 20 healthy controls (38). The authors found that the T1 mapping technique was possible in 90% of the subjects. The most appropriate imaging plane was the mid-ventricular short-axis view, and systole was preferred over diastole given the larger amount of myocardium that could be evaluated during systole. Interestingly, the average T1 time of the RV myocardium was significantly longer than the LV myocardium. The authors believed this was due to the naturally higher collagen content in the RV.

Higher resolution T1 mapping sequences, which may be more appropriate for the thin-walled RV myocardium, are in development. Recently, an accelerated and navigator-gated look-locker imaging sequence (ANGIE) was developed for T1 quantification of the RV (37). The authors found that ANGIE provided lower intra-scan variability compared to standard MOLLI with clinically reasonable scan times.

Another high-resolution T1 mapping sequence under development is similar to standard MOLLI but the interpolated spatial resolution is reduced from 1.4 x 1.4 mm to 0.5 x 0.5 mm. (Figure 3). Although results are still preliminary, this technique has the potential to detect diffuse fibrosis of the RV in heart failure. Given the importance of RV health in patients with PH, T1 mapping (i.e., the amount of diffuse RV myocardial fibrosis) may serve as a novel tool for measuring therapeutic success in PH.

Right ventricular strain imaging

CMR has the advantage of flexible 2D slice prescription, as well as the potential for volumetric coverage of the whole heart. The quantitative evaluation of regional myocardial function using strain imaging has the potential to improve the sensitivity of CMR to regional decrements in RV function that may precede global changes in the RV systolic function. The majority of available literature for RV analysis reports longitudinal and circumferential strains, given the limited amount of radial RV strain due to the thin RV myocardium.

Myocardial strain can be calculated using several different CMR techniques. Myocardial tagging is the most studied, well-validated technique for assessing myocardial strain. Challenges to myocardial tagging of the RV include the wall thickness relative to tag spacing and time-intensive analysis (39). Harmonic phase analysis (HARP) is a post-processing technique which tracks pixels on time-resolved tagging images, applying a constant phase constraint (40); this technique streamlines tag analysis. Displacement encoding with stimulated echoes (DENSE) (41), strain encoded imaging (SENC) (42), deformation field analysis, and multimodality feature tracking (43) have also been applied to measure RV strain. DENSE directly encodes tissue displacement into the image phase by encoding and decoding gradients. The resultant stimulated echo fades secondary to T1 recovery limiting assessment of mid to late diastolic strains. SENC shares similarities with DENSE and tagging, but differs through application of tag lines parallel to the imaging plane. Myocardial deformation analysis and feature tracking are unique in that they are applied to bSSFP cine image data, yielding strain data without the need for dedicated image acquisitions. The majority of work evaluating the utility of RV strain analysis on CMR has focused on myocardial tagging, HARP, or SENC techniques. Several feature tracking software systems are available, with differing algorithms for identifying and tracking endo-, epi-, and intramyocardial image features over time with promising results for assessment of RV strain (43).

Strain analysis on cardiac MRI has focused on identifying early changes in RV function that precede maladaptive RV remodeling (44). Shehata et al. evaluated segmental RV myocardial strains using fast SENC in a cohort of 35 patients with PAH, demonstrating reduced RV longitudinal strain in nearly all segments, with reduced RV circumferential strain in the mid chamber (45).. Importantly, in a subgroup analysis of 13 patients with PAH and preserved RV ejection fraction (51–61%), segmentally reduced longitudinal strain was demonstrated in the RV basal- and mid-chamber anteroseptal and RV mid-chamber anterior segments compared to a cohort of healthy controls, indicating the ability to detect regional changes in function prior to reductions in global RV ejection fraction. Myocardial strain imaging has also been used to identify ventricular dyssynchrony in PH using myocardial tagging by determining differences in time to peak RV and LV circumferential strains (46). For example, ventricular dyssynchrony assessed by myocardial tagging has been shown to normalize following thromboendarterectomy in patients with chronic thromboembolic pulmonary hypertension (CTEPH) (46).

Right ventricular perfusion

A critical component of RV failure in PH is a decline in coronary perfusion of the RV and subsequent RV ischemia. Coronary blood flow can be evaluated by CMR using gadolinium contrast and a coronary vasodilator such as adenosine or regadenoson, and also by PC-MRI techniques. In an earlier study involving PC-MRI, Van Wolferen et al. found that right coronary artery peak and mean systolic flow in PAH patients was significantly decreased compared to controls (47) (Figure 4). These changes correlated inversely with RV mass and RV pressure. The results of this study help explain the effects of PH and a failing RV on coronary blood flow.

In a subsequent study of 25 patients referred for PAH evaluation, myocardial perfusion reserve index was evaluated using CMR for both the LV and RV and found to be significantly decreased compared to controls (48). The potential to non-invasively calculate RV blood flow in patients with PH may serve to guide the initiation and/or effectiveness of PH therapies.

Pulmonary artery 4D flow imaging

Functional characterization of the PAs is increasingly important given that PH is not merely a disease of the distal vessels, as the proximal PAs undergo dilation, remodeling, and stiffening. The distal and proximal PA changes not only contribute to decreased compliance and increased resistance thereby increasing RV afterload, but also alter secondary flows (such as helix and vortex formation) including changes to the velocity profile shape and magnitude (49–51). To this end, PC-MRI can be employed to assess cardiovascular hemodynamics and quantify blood flow velocities in the main PAs, the RV and the RV outflow tract. In addition, PC-MRI data has been used to derive more advanced hemodynamic metrics such as pulse wave velocity (which can characterize arterial stiffness), vorticity (which may detect diastolic RV dysfunction), and wall shear stress (WSS; which regulates endothelial cell function and vascular remodeling) (52–54).

More recently, a number of studies have employed 4D flow MRI (time-resolved 3D phase-contrast MRI with three-directional velocity encoding), which offers the opportunity to non-invasively measure complex 3D hemodynamic changes with full volumetric coverage of the RV and PAs (49,55,56) (Figure 5). A recent study has confirmed that volumetric analysis based on 4D flow MRI allows for improved assessment of aortic and pulmonary peak velocities, which may be underestimated by both Doppler echocardiography and 2D PC MRI, which are limited by 2D analysis planes and single-directional velocity encoding (57). Moreover, a number of studies have demonstrated low inter-observer variability, high test-retest reliability, and good correlation between flow parameters obtained by 4D flow MRI and 2D cine PC MRI (58–60).

Using 4D flow MRI in the pulmonary circulation, Reiter et al. (49,50) observed abnormal vortex development in the main PA in patients with PAH, resulting in an abnormal boundary layer along the wall of the main PA. Notably, the time persistence of this vortex correlated with the degree of PH as measured by mean PA pressure (mPAP) (50). 4D flow MRI and 3D flow visualization in the PAs may have the potential to provide a non-invasive vortex-based

diagnosis of PH. François et al. (55) and Geiger et al. (61) similarly observed increased vortex flow patterns in the PAs of patients with repaired tetralogy of Fallot. Another recent 4D flow study in a canine model of acute thromboembolic PH demonstrated that right and left ventricular function, PA flow, tricuspid valve regurgitation velocity, and aorta flow could be quantified based on a single 4D flow MRI exam (62). Fenster et al. recently correlated complex RV vortex flow with multiple echocardiographic markers of RV diastolic dysfunction (53). In particular trans-tricuspid valve E and A velocities, E/A ratio, and e' and a' tissue Doppler velocities were all significantly correlated with degree of vorticity.

We are only beginning to understand the role of the complex flow changes documented in these investigational studies for PH diagnosis and monitoring progression. One direct application of 4D flow MRI to PH may be WSS, a parameter known to stimulate vasodilation via nitric oxide release from endothelial cells, vascular remodeling, and intrinsic proximal vessel characteristics (51,63,64). In this respect, 4D flow is a highly informative tool, given that altered 3D flow is not focal to the RV but is also present in the enlarged PAs of PAH patients (49,50). Proximal PA stiffening and dilation as a result of collagen accumulation (or elastin loss) and pressure loading will diminish the Windkessel effect and alter the function of the dual stage RV-PA unit (65,66). It is presumed that this phenomenon increases RV afterload and alters proximal as well as distal flow dynamics. The changes can be measured in the form of bulk flow (SV, cardiac output, Q_{max}) as well as in the form of maximum velocity and WSS. Indeed, a recent 4D flow MRI study was able to detect differences in PA hemodynamics in patients with PAH (67). V_{max}, Q_{max}, SV, and WSS at all locations were significantly lower ($p<0.05$) in PAH compared to healthy subjects. These investigational 4D flow studies extend our understanding of the changes occurring to structure and flow in the presence of the hypertensive RV and PAs and how they may possibly affect the progression of the various forms of PH and response to therapy.

Integration of magnetic resonance imaging and invasive hemodynamic testing

While MRI imaging can provide a comprehensive assessment of the RV and pulmonary vasculature in PH patients (as summarized in Table 2), the combination of invasive hemodynamic data, obtained during right heart catheterization, and main PA cross-sectional area can allow for the calculation of several indices of proximal PA stiffness, such as PA compliance, distensibility, elastic modulus, and stiffness index (β) (23,24) (Table 3). Increased proximal PA stiffness (i.e., reduced proximal PA compliance) occurs in virtually all etiologies of PH and can contribute to RV dysfunction. The PA pulsatility and relative area change measures (described above) are not true measures of PA compliance, although they are valid surrogates of PA compliance measures. Combining PA cross-sectional area change with invasive hemodynamic data can provide the aforementioned PA compliance measures such as the PA stiffness index β. Sanz et al. calculated proximal PA stiffness measures in 94 patients who underwent both CMR and invasive hemodynamic testing, and divided the patients into those with no PH (controls), exercise-induced PH (i.e., early PH), and PH at rest (23). These authors found that proximal PA stiffness increased early in PH patients compared to controls, thereby providing mechanistic insight into the development of PH. It is interesting to note, however, that an acute increase in pressure can also increase proximal PA stiffness via strain-stiffening, as recently demonstrated in a canine model of

acute PH (24). Thus, whether increased proximal PA stiffness (and decreased PA compliance) with PH are due to remodeling or strain remains unclear.

COMPUTED TOMOGRAPHY: CURRENT APPROACHES IN PULMONARY HYPERTENSION

Diagnostic role of computed tomography in pulmonary hypertension

Non-contrast computed tomography (NCCT) and computed tomography angiography (CTA) are the two main CT techniques that have a significant role in the clinical evaluation and management of patients with PH. The pulmonary parenchymal findings on CT in patients with PH are variable and depend upon the etiology. NCCT is sufficient for the evaluation of most lung diseases given its ability to accurately identify structural changes in the airways and parenchyma. Specifically, NCCT is indicated for (a) the evaluation of the lung parenchyma in diffuse lung diseases such as chronic obstructive pulmonary disease and interstitial lung diseases; (b) the detection of pulmonary arteriovenous malformations; and (c) the diagnosis of pulmonary veno-occlusive disease or pulmonary capillary hemangiomatosis. Table 4 lists CT findings that are useful for the diagnosis of PH and underlying PH etiologies on NCCT.

CTA, which requires the intravenous administration of iodinated contrast material, has become the reference standard for the diagnosis of acute pulmonary embolism given its ability to routinely assess PAs to the subsegmental level; however, the role of CTA to screen for chronic pulmonary emboli in PH is less well established. Although CTA is not indicated in the primary imaging evaluation of PH, there are secondary signs present on CTA studies that are suggestive of PH and provide additional prognostic information, that are described below.

Qualitative and quantitative computed tomography findings in pulmonary hypertension

The most conspicuous finding on both NCCT and CTA suggestive of PH is dilation of the central PAs (Figure 6). Other findings of PH present on both NCCT and CTA include PA calcification, tortuosity of the PAs, rapid tapering of the PAs, and mosaic attenuation of the lung parenchyma (Figure 6). Additional findings of PH on CTA include reflux of intravenous contrast into the hepatic veins, RV dilation, RV hypertrophy, flattening or bowing of the IVS, and dilation of the bronchial arteries. Chan et al. published data from a retrospective study in hospitalized patients that underwent both CT and invasive hemodynamic testing during the same hospitalization and found a variety of CT-based indices to be significantly correlated with elevated invasively-measured PA pressures (68). In addition to main PA diameter and main PA-to-ascending aorta diameter ratio, these investigators found that descending right and left PA diameter, RV wall thickness, RV/LV wall thickness ratio, and RV/LV diameter ratios were also highly associated with PH (68).

COMPUTED TOMOGRAPHY: NOVEL APPROACHES IN PULMONARY HYPERTENSION

One of the greatest unmet needs in PH imaging is the ability to characterize the distal pulmonary vasculature in PH—particularly PAH, which is thought to be a disease of the small pulmonary arteries. Newer CT scanners have implemented methods of performing dual-energy CT (DECT), enabling the ability to quantitatively characterize the material properties of soft tissues, including the distal pulmonary vasculature, with CT (Figure 7). There are two main DECT technologies available, one that uses two x-ray sources and detector (dual source CT [DSCT]) and one that uses a single x-ray source and detector. DSCT and DECT with rapid kilovoltage switching methods have been investigated in PH and have shown promise in their ability to generate quantitative lung perfusion and pulmonary blood volume maps using the same acquisition that would be used for standard pulmonary CTA (69).

STRENGTHS AND WEAKNESS OF ECHOCARDIOGRAPHY, MAGNETIC RESONANCE IMAGING, AND COMPUTED TOMOGRAPHY FOR THE EVALUATION OF PULMONARY HYPERTENSION

While the strengths of both CMR and CT relative to echocardiography are detailed in this review, there are a number of drawbacks for each imaging modality that are worth mentioning.

Echocardiography is the mainstay of screening and initial assessment of PH given its low cost, widespread availability, and potential for bedside application. In addition, 2D echocardiography is performed in real-time and has a much higher frame rate than either MRI or CT and remains the gold standard for non-invasive hemodynamic assessment. Nevertheless, sonographer technique, acoustic windows, and non-tomographic views are all factors that can limit its utility in the individual patient.

The major weakness of NCCT and CTA is the need for ionizing radiation. An additional disadvantage of CTA is the need for iodinated contrast material administration. However, with newer multi-slice scanners and iterative reconstruction techniques, the overall radiation dose and amount of contrast needed continues to improve.

For MRI, the acquisition time continues to be lengthy despite a number of technical advancements that allow for fewer breath-holds. MRI also requires technical expertise and occasional time-consuming post-processing. PH patients receiving subcutaneous or intravenous prostacyclin treatment can be scanned, but ensuring the safety and monitoring of these patients can increase MRI acquisition time and the requirement for specialized personnel. In addition, gadolinium-based contrast is relatively contraindicated in patients with a glomerular filtration rate < 30 ml/min/1.73 m^2; however, many of the sequences used in PH (standard cines for RV size and function, velocity-encoded imaging for PA flow, and even 4D flow) do not require contrast.

One common misconception is that cost is always a major limitation for MRI and CT. Although overall cost is higher than echocardiography, the total cost is dependent on the type of MRI/CT used and whether or not contrast is given. The cost of NCCT, for instance, is only slightly higher than echocardiography while the cost of MRI without contrast is similar to trans-esophageal echocardiography (Table 5).

The role of computed tomography and magnetic resonance imaging in pulmonary hypertension clinical trials

Since the pivotal clinical trial of epoprostenol in 1996, the 6-minute walk distance (6MWD) test has been the accepted exercise endpoint for studies evaluating the treatment effects of PAH in adults. Although measurable, non-invasive, easy to obtain, and cost-effective, 6MWD provides little insight into the mechanism of therapeutic action. In addition, what constitutes a relevant change in 6MWD is complex and not necessarily clinically meaningful despite statistical significance. An ideal surrogate should be able to predict clinically meaningful outcomes (70).

The response of the RV to increased afterload is the greatest determinant of a PH patient's symptoms and survival; therefore, parameters of RV function may be the ideal surrogate endpoints for future PH clinical trials. CMR, in particular, is well-suited for providing these parameters. Although cost-effectiveness is thought to be a major barrier for using CMR in clinical studies, Addetia et al. showed that the superior reproducibility of CMR in measuring RV volumes and function allowed for lower overall global fees compared to echocardiography due to the fact that fewer subjects were needed to detect changes in these measurements (71).

A number of small randomized controlled trials and prospective non-randomized (observational) trials have already explored the use of CMR in PH (Table 6). Although these studies show that CMR can be used effectively in clinical trials, more work is needed to examine the clinical relevance of changes in these CMR parameters.

VALUE-BASED IMAGING FOR PULMONARY HYPERTENSION

As reimbursement patterns change in response to the rising costs of healthcare, it is clear that there will be a shift in incentives from volume-based to value-based imaging strategies, and the imaging of PH will be no exception to this rule. In line with these initiatives is the acknowledgement that quality and safety are of cardinal importance when selecting and performing imaging in all patients, including those with PH. Several strategies have been employed to increase the value of cardiovascular imaging overall; these include appropriateness criteria, accreditation, quality measurement, technical standards, and practice guidelines.

The imaging of PH patients is a perfect example of a clinical syndrome that can result in a high volume of imaging tests: echocardiograms, both at baseline and repeated over time, coupled with CT, MRI, and nuclear scans, not to mention a battery of other tests, including invasive hemodynamic and cardiopulmonary exercise testing, occur in a large number of these patients. In the future, healthcare providers will need to be much more judicious in

their use of these imaging tests in order to improve both value and patient experience while keeping costs down. Furthermore, the quality of advanced imaging modalities—particularly MRI—can be quite variable. Therefore, centers of excellence for MRI imaging of complex disease states such as PH may be necessary in order to improve the value and yield of imaging tests.

An efficient algorithm for the approach to imaging of the PH patient may reduce costs and improve value. We present one such algorithm (Figure 8), which takes advantage of the fact that the majority of patients with PH have left heart disease. For example, by screening for left heart disease with echocardiography, treating, and then re-imaging with echocardiography, many patients may not require further imaging tests. While algorithms such as those presented in Figure 8 may be attractive initiatives in the era of cost containment, only randomized controlled trials of imaging algorithms vs. usual care will determine whether value-based imaging strategies will truly improve patient outcomes, enhance the patient experience, and decrease costs in patients with PH.

CONCLUSIONS

MRI and CT imaging modalities are capable of determining the etiology and pathophysiology of PH, and can be extremely useful in the management of these patients. Advances in these imaging modalities are occurring at a rapid pace, with exciting new techniques such as RV tissue characterization with T1 mapping, 4D flow of the RV and PAs, and CT lung perfusion imaging paving the way for a new era of imaging in PH patients. These imaging modalities complement echocardiography and invasive hemodynamic testing, and may be useful as surrogate endpoints for early-phase PH clinical trials. While the costs of MRI and CT continue to come down, it is important to recognize that a high volume of imaging tests is not appropriate, and the transition from volume-based to value-based imaging is on the horizon. By understanding the optimal techniques and indications for MRI and CT in PH, health care providers will be able to judiciously use these imaging tests, thereby increasing value and decreasing overall costs.

Acknowledgments

FUNDING SOURCES

B.H.F. is funded by research grants from the International Society of Heart and Lung Transplantation and Northwestern Memorial Foundation; J.D.C. is funded by research grants from the RSNA Research and Education Foundation, the Society of Interventional Radiology Foundation, and Bard Access Systems; N.C.C. is funded by research grants from the National Institutes of Health (R01 HL086939 and R01 HL105598); M.M. is funded by research grants from the National Institutes of Health (R01 HL115828 and R01 HL117888); A.J.B is funded by a research grants from the National Institutes of Health (K25HL119608); and S.J.S. is funded by research grants from the National Institutes of Health (R01 HL107557 and R01 HL127028), Actelion, and Novartis.

ABBREVIATIONS

ANGIE	accelerated and navigator-gated look-locker imaging sequence
bSSFP	balanced steady state free precession
DENSE	displacement encoding with stimulated echoes

HARP	harmonic phase analysis
MOLLI	modified look-locker inversion
NCCT	non-contrast computed tomography
PC	phase contrast
RVIP	right ventricular insertion point
SENC	strain encoded imaging
WSS	wall shear stress

References

1. McLaughlin VV, Shah SJ, Souza R, Humbert M. Management of pulmonary arterial hypertension. J Am Coll Cardiol. 2015; 65:1976–97. [PubMed: 25953750]
2. Shah SJ. Pulmonary hypertension. JAMA. 2012; 308:1366–74. [PubMed: 23032553]
3. Peacock AJ, Crawley S, McLure L, et al. Changes in right ventricular function measured by cardiac magnetic resonance imaging in patients receiving pulmonary arterial hypertension-targeted therapy: the EURO-MR study. Circ Cardiovasc Imaging. 2014; 7:107–14. [PubMed: 24173272]
4. Grothues F, Moon JC, Bellenger NG, Smith GS, Klein HU, Pennell DJ. Interstudy reproducibility of right ventricular volumes, function, and mass with cardiovascular magnetic resonance. Am Heart J. 2004; 147:218–23. [PubMed: 14760316]
5. Grothues F, Smith GC, Moon JC, et al. Comparison of interstudy reproducibility of cardiovascular magnetic resonance with two-dimensional echocardiography in normal subjects and in patients with heart failure or left ventricular hypertrophy. Am J Cardiol. 2002; 90:29–34. [PubMed: 12088775]
6. Jauhiainen T, Jarvinen VM, Hekali PE. Evaluation of methods for MR imaging of human right ventricular heart volumes and mass. Acta Radiol. 2002; 43:587–92. [PubMed: 12485256]
7. Hori Y, Yamada N, Higashi M, Hirai N, Nakatani S. Rapid evaluation of right and left ventricular function and mass using real-time true-FISP cine MR imaging without breath-hold: comparison with segmented true-FISP cine MR imaging with breath-hold. J Cardiovasc Magn Reson. 2003; 5:439–50. [PubMed: 12882075]
8. Peacock AJ, Vonk Noordegraaf A. Cardiac magnetic resonance imaging in pulmonary arterial hypertension. Eur Respir Rev. 2013; 22:526–34. [PubMed: 24293468]
9. van Wolferen SA, van de Veerdonk MC, Mauritz GJ, et al. Clinically significant change in stroke volume in pulmonary hypertension. Chest. 2011; 139:1003–9. [PubMed: 20864614]
10. Buckberg GD, Group R. The ventricular septum: the lion of right ventricular function, and its impact on right ventricular restoration. Eur J Cardiothorac Surg. 2006; 29(Suppl 1):S272–8. [PubMed: 16567103]
11. Gan C, Lankhaar JW, Marcus JT, et al. Impaired left ventricular filling due to right-to-left ventricular interaction in patients with pulmonary arterial hypertension. Am J Physiol Heart Circ Physiol. 2006; 290:H1528–33. [PubMed: 16284226]
12. Marcus JT, Gan CT, Zwanenburg JJ, et al. Interventricular mechanical asynchrony in pulmonary arterial hypertension: left-to-right delay in peak shortening is related to right ventricular overload and left ventricular underfilling. J Am Coll Cardiol. 2008; 51:750–7. [PubMed: 18279740]
13. Haddad F, Guihaire J, Skhiri M, et al. Septal curvature is marker of hemodynamic, anatomical, and electromechanical ventricular interdependence in patients with pulmonary arterial hypertension. Echocardiography. 2014; 31:699–707. [PubMed: 24372843]
14. Roeleveld RJ, Marcus JT, Faes TJ, et al. Interventricular septal configuration at mr imaging and pulmonary arterial pressure in pulmonary hypertension. Radiology. 2005; 234:710–7. [PubMed: 15634939]

15. Alunni JP, Degano B, Arnaud C, et al. Cardiac MRI in pulmonary artery hypertension: correlations between morphological and functional parameters and invasive measurements. Eur Radiol. 2010; 20:1149–59. [PubMed: 20094890]
16. Sciancalepore MA, Maffessanti F, Patel AR, et al. Three-dimensional analysis of interventricular septal curvature from cardiac magnetic resonance images for the evaluation of patients with pulmonary hypertension. Int J Cardiovasc Imaging. 2012; 28:1073–85. [PubMed: 21695484]
17. Sato T, Tsujino I, Ohira H, et al. Paradoxical interventricular septal motion as a major determinant of late gadolinium enhancement in ventricular insertion points in pulmonary hypertension. PLoS One. 2013; 8:e66724. [PubMed: 23826118]
18. Pelc NJ, Sommer FG, Li KCP, Brosnan TJ, Herfkens RJ, Enzmann DR. Quantitative Magnetic-Resonance Flow Imaging. Magn Reson Q. 1994; 10:125–147. [PubMed: 7811608]
19. Ley S, Mereles D, Puderbach M, et al. Value of MR phase-contrast flow measurements for functional assessment of pulmonary arterial hypertension. European Radiology. 2007; 17:1892–1897. [PubMed: 17225131]
20. Kondo C, Caputo GR, Masui T, et al. Pulmonary-Hypertension - Pulmonary Flow Quantification and Flow Profile Analysis with Velocity-Encoded Cine Mr Imaging. Radiology. 1992; 183:751–758. [PubMed: 1584932]
21. Mousseaux E, Tasu JP, Jolivet O, Simonneau G, Bittoun J, Gaux JC. Pulmonary arterial resistance: Noninvasive measurement with indexes of pulmonary flow estimated at velocity-encoded MR imaging - Preliminary experience. Radiology. 1999; 212:896–902. [PubMed: 10478263]
22. Bogren HG, Klipstein RH, Mohiaddin RH, et al. Pulmonary-Artery Distensibility and Blood-Flow Patterns - a Magnetic-Resonance Study of Normal Subjects and of Patients with Pulmonary Arterial-Hypertension. Am Heart J. 1989; 118:990–999. [PubMed: 2816711]
23. Sanz J, Kariisa M, Dellegrottaglie S, et al. Evaluation of pulmonary artery stiffness in pulmonary hypertension with cardiac magnetic resonance. JACC Cardiovasc Imaging. 2009; 2:286–95. [PubMed: 19356573]
24. Bellofiore A, Chesler NC. Methods for measuring right ventricular function and hemodynamic coupling with the pulmonary vasculature. Ann Biomed Eng. 2013; 41:1384–98. [PubMed: 23423705]
25. Gan CT, Lankhaar JW, Westerhof N, et al. Noninvasively assessed pulmonary artery stiffness predicts mortality in pulmonary arterial hypertension. Chest. 2007; 132:1906–12. [PubMed: 17989161]
26. Ohno Y, Hatabu H, Murase K, et al. Primary pulmonary hypertension: 3D dynamic perfusion MRI for quantitative analysis of regional pulmonary perfusion. AJR Am J Roentgenol. 2007; 188:48–56. [PubMed: 17179345]
27. Ohno Y, Murase K, Higashino T, et al. Assessment of bolus injection protocol with appropriate concentration for quantitative assessment of pulmonary perfusion by dynamic contrast-enhanced MR imaging. J Magn Reson Imaging. 2007; 25:55–65. [PubMed: 17152051]
28. Swift AJ, Wild JM, Nagle SK, et al. Quantitative magnetic resonance imaging of pulmonary hypertension: a practical approach to the current state of the art. J Thorac Imaging. 2014; 29:68–79. [PubMed: 24552882]
29. Sanz J, Garcia-Alvarez A, Fernandez-Friera L, et al. Right ventriculo-arterial coupling in pulmonary hypertension: a magnetic resonance study. Heart. 2012; 98:238–43. [PubMed: 21917658]
30. Freed BH, Gomberg-Maitland M, Chandra S, et al. Late gadolinium enhancement cardiovascular magnetic resonance predicts clinical worsening in patients with pulmonary hypertension. J Cardiovasc Magn Reson. 2012; 14:11. [PubMed: 22296860]
31. Shehata ML, Lossnitzer D, Skrok J, et al. Myocardial delayed enhancement in pulmonary hypertension: pulmonary hemodynamics, right ventricular function, and remodeling. AJR Am J Roentgenol. 2011; 196:87–94. [PubMed: 21178051]
32. Vogel-Claussen J, Shehata ML, Lossnitzer D, et al. Increased right ventricular Septomarginal trabeculation mass is a novel marker for pulmonary hypertension: comparison with ventricular mass index and right ventricular mass. Invest Radiol. 2011; 46:567–75. [PubMed: 21577127]

33. Mewton N, Liu CY, Croisille P, Bluemke D, Lima JA. Assessment of myocardial fibrosis with cardiovascular magnetic resonance. J Am Coll Cardiol. 2011; 57:891–903. [PubMed: 21329834]
34. Iles L, Pfluger H, Phrommintikul A, et al. Evaluation of diffuse myocardial fibrosis in heart failure with cardiac magnetic resonance contrast-enhanced T1 mapping. J Am Coll Cardiol. 2008; 52:1574–80. [PubMed: 19007595]
35. Won S, Davies-Venn C, Liu S, Bluemke DA. Noninvasive imaging of myocardial extracellular matrix for assessment of fibrosis. Curr Opin Cardiol. 2013; 28:282–9. [PubMed: 23549230]
36. Garcia-Alvarez A, Garcia-Lunar I, Pereda D, et al. Association of myocardial T1-mapping CMR with hemodynamics and RV performance in pulmonary hypertension. JACC Cardiovasc Imaging. 2015; 8:76–82. [PubMed: 25592698]
37. Mehta BB, Chen X, Bilchick KC, Salerno M, Epstein FH. Accelerated and navigator-gated look-locker imaging for cardiac t1 estimation (ANGIE): Development and application to T1 mapping of the right ventricle. Magn Reson Med. 2014
38. Kawel-Boehm N, Dellas Buser T, Greiser A, Bieri O, Bremerich J, Santini F. In-vivo assessment of normal T1 values of the right-ventricular myocardium by cardiac MRI. Int J Cardiovasc Imaging. 2014; 30:323–8. [PubMed: 24221905]
39. Tee M, Noble JA, Bluemke DA. Imaging techniques for cardiac strain and deformation: comparison of echocardiography, cardiac magnetic resonance and cardiac computed tomography. Expert Rev Cardiovasc Ther. 2013; 11:221–31. [PubMed: 23405842]
40. Osman NF, Kerwin WS, McVeigh ER, Prince JL. Cardiac motion tracking using CINE harmonic phase (HARP) magnetic resonance imaging. Magn Reson Med. 1999; 42:1048–60. [PubMed: 10571926]
41. Aletras AH, Ingkanisorn WP, Mancini C, Arai AE. DENSE with SENSE. J Magn Reson. 2005; 176:99–106. [PubMed: 15946874]
42. Freed BH, Tsang W, Bhave NM, et al. Right ventricular strain in pulmonary arterial hypertension: a 2D echocardiography and cardiac magnetic resonance study. Echocardiography. 2015; 32:257–63. [PubMed: 24975738]
43. Schuster A, Morton G, Hussain ST, et al. The intra-observer reproducibility of cardiovascular magnetic resonance myocardial feature tracking strain assessment is independent of field strength. Eur J Radiol. 2013; 82:296–301. [PubMed: 23246014]
44. Meris A, Faletra F, Conca C, et al. Timing and magnitude of regional right ventricular function: a speckle tracking-derived strain study of normal subjects and patients with right ventricular dysfunction. J Am Soc Echocardiogr. 2010; 23:823–31. [PubMed: 20646910]
45. Shehata ML, Harouni AA, Skrok J, et al. Regional and global biventricular function in pulmonary arterial hypertension: a cardiac MR imaging study. Radiology. 2013; 266:114–22. [PubMed: 23151825]
46. Mauritz GJ, Vonk-Noordegraaf A, Kind T, et al. Pulmonary endarterectomy normalizes interventricular dyssynchrony and right ventricular systolic wall stress. J Cardiovasc Magn Reson. 2012; 14:5. [PubMed: 22240072]
47. van Wolferen SA, Marcus JT, Westerhof N, et al. Right coronary artery flow impairment in patients with pulmonary hypertension. Eur Heart J. 2008; 29:120–7. [PubMed: 18065750]
48. Vogel-Claussen J, Skrok J, Shehata ML, et al. Right and left ventricular myocardial perfusion reserves correlate with right ventricular function and pulmonary hemodynamics in patients with pulmonary arterial hypertension. Radiology. 2011; 258:119–27. [PubMed: 20971775]
49. Reiter G, Reiter U, Kovacs G, et al. Magnetic resonance-derived 3-dimensional blood flow patterns in the main pulmonary artery as a marker of pulmonary hypertension and a measure of elevated mean pulmonary arterial pressure. Circ Cardiovasc Imaging. 2008; 1:23–30. [PubMed: 19808511]
50. Reiter U, Reiter G, Kovacs G, et al. Evaluation of elevated mean pulmonary arterial pressure based on magnetic resonance 4D velocity mapping: comparison of visualization techniques. PLoS One. 2013; 8:e82212. [PubMed: 24349224]
51. Truong U, Fonseca B, Dunning J, et al. Wall shear stress measured by phase contrast cardiovascular magnetic resonance in children and adolescents with pulmonary arterial hypertension. J Cardiovasc Magn Reson. 2013; 15:81. [PubMed: 24034144]

52. Chien S, Li S, Shyy YJ. Effects of mechanical forces on signal transduction and gene expression in endothelial cells. Hypertension. 1998; 31:162–9. [PubMed: 9453297]
53. Fenster BE, Browning J, Schroeder JD, et al. Vorticity is a Marker of Right Ventricular Diastolic Dysfunction. Am J Physiol Heart Circ Physiol. 2015 ajpheart 00278 2015.
54. Kopec G, Moertl D, Jankowski P, Tyrka A, Sobien B, Podolec P. Pulmonary artery pulse wave velocity in idiopathic pulmonary arterial hypertension. Can J Cardiol. 2013; 29:683–90. [PubMed: 23260799]
55. Francois CJ, Srinivasan S, Schiebler ML, et al. 4D cardiovascular magnetic resonance velocity mapping of alterations of right heart flow patterns and main pulmonary artery hemodynamics in tetralogy of Fallot. J Cardiovasc Magn Reson. 2012; 14:16. [PubMed: 22313680]
56. Fredriksson AG, Zajac J, Eriksson J, et al. 4-D blood flow in the human right ventricle. Am J Physiol Heart Circ Physiol. 2011; 301:H2344–50. [PubMed: 21926347]
57. Nordmeyer S, Riesenkampff E, Messroghli D, et al. Four-dimensional velocity-encoded magnetic resonance imaging improves blood flow quantification in patients with complex accelerated flow. J Magn Reson Imaging. 2013; 37:208–16. [PubMed: 22976284]
58. Nordmeyer S, Riesenkampff E, Crelier G, et al. Flow-sensitive four-dimensional cine magnetic resonance imaging for offline blood flow quantification in multiple vessels: a validation study. J Magn Reson Imaging. 2010; 32:677–83. [PubMed: 20815066]
59. Markl M, Wallis W, Harloff A. Reproducibility of flow and wall shear stress analysis using flow-sensitive four-dimensional MRI. J Magn Reson Imaging. 2011; 33:988–94. [PubMed: 21448968]
60. Frydrychowicz A, Wieben O, Niespodzany E, Reeder SB, Johnson KM, Francois CJ. Quantification of Thoracic Blood Flow Using Volumetric Magnetic Resonance Imaging With Radial Velocity Encoding: In Vivo Validation. Invest Radiol. 2013
61. Geiger J, Markl M, Jung B, et al. 4D-MR flow analysis in patients after repair for tetralogy of Fallot. Eur Radiol. 2011; 21:1651–7. [PubMed: 21720942]
62. Roldan-Alzate A, Frydrychowicz A, Johnson KM, et al. Non-invasive assessment of cardiac function and pulmonary vascular resistance in an canine model of acute thromboembolic pulmonary hypertension using 4D flow cardiovascular magnetic resonance. J Cardiovasc Magn Reson. 2014; 16:23. [PubMed: 24625242]
63. Tang BT, Pickard SS, Chan FP, Tsao PS, Taylor CA, Feinstein JA. Wall shear stress is decreased in the pulmonary arteries of patients with pulmonary arterial hypertension: An image-based, computational fluid dynamics study. Pulm Circ. 2012; 2:470–6. [PubMed: 23372931]
64. Wang Z, Lakes RS, Golob M, Eickhoff JC, Chesler NC. Changes in large pulmonary arterial viscoelasticity in chronic pulmonary hypertension. PLoS One. 2013; 8:e78569. [PubMed: 24223157]
65. Lammers SR, Kao PH, Qi HJ, et al. Changes in the structure-function relationship of elastin and its impact on the proximal pulmonary arterial mechanics of hypertensive calves. Am J Physiol Heart Circ Physiol. 2008; 295:H1451–H1459. [PubMed: 18660454]
66. Kobs RW, Muvarak NE, Eickhoff JC, Chesler NC. Linked mechanical and biological aspects of remodeling in mouse pulmonary arteries with hypoxia-induced hypertension. Am J Physiol Heart Circ Physiol. 2005; 288:H1209–17. [PubMed: 15528223]
67. Barker AJ, Roldan-Alzate A, Entezari P, et al. Four-dimensional flow assessment of pulmonary artery flow and wall shear stress in adult pulmonary arterial hypertension: results from two institutions. Magn Reson Med. 2015; 73:1904–13. [PubMed: 24974951]
68. Chan AL, Juarez MM, Shelton DK, et al. Novel computed tomographic chest metrics to detect pulmonary hypertension. BMC Med Imaging. 2011; 11:7. [PubMed: 21447184]
69. Dournes G, Verdier D, Montaudon M, et al. Dual-energy CT perfusion and angiography in chronic thromboembolic pulmonary hypertension: diagnostic accuracy and concordance with radionuclide scintigraphy. Eur Radiol. 2014; 24:42–51. [PubMed: 23982287]
70. Gomberg-Maitland M, Bull TM, Saggar R, et al. New trial designs and potential therapies for pulmonary artery hypertension. J Am Coll Cardiol. 2013; 62:D82–91. [PubMed: 24355645]
71. Addetia K, Bhave NM, Tabit CE, et al. Sample size and cost analysis for pulmonary arterial hypertension drug trials using various imaging modalities to assess right ventricular size and function end points. Circ Cardiovasc Imaging. 2014; 7:115–24. [PubMed: 24192452]

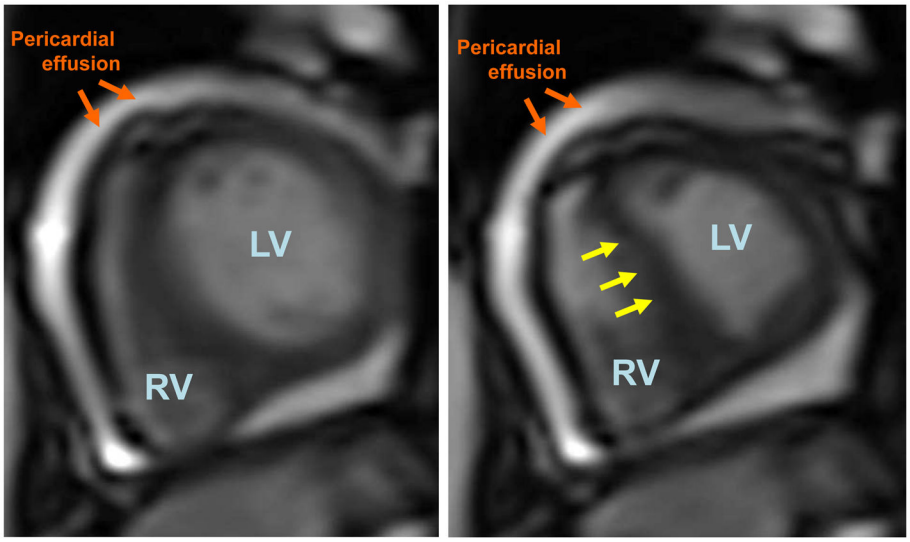

Figure 1. Dynamic interventricular septal shift from right to left in a patient with systemic sclerosis-associated pulmonary arterial hypertension on cardiac magnetic resonance imaging

LV = left ventricular; RV = right ventricular. Yellow arrows point to interventricular septal shift during inspiration.

Figure 2. Late gadolinium enhancement at the right ventricle insertion points in a patient with pulmonary arterial hypertension on cardiac magnetic resonance imaging

Arrows point to late gadolinium contrast enhancement at right ventricular insertion points.

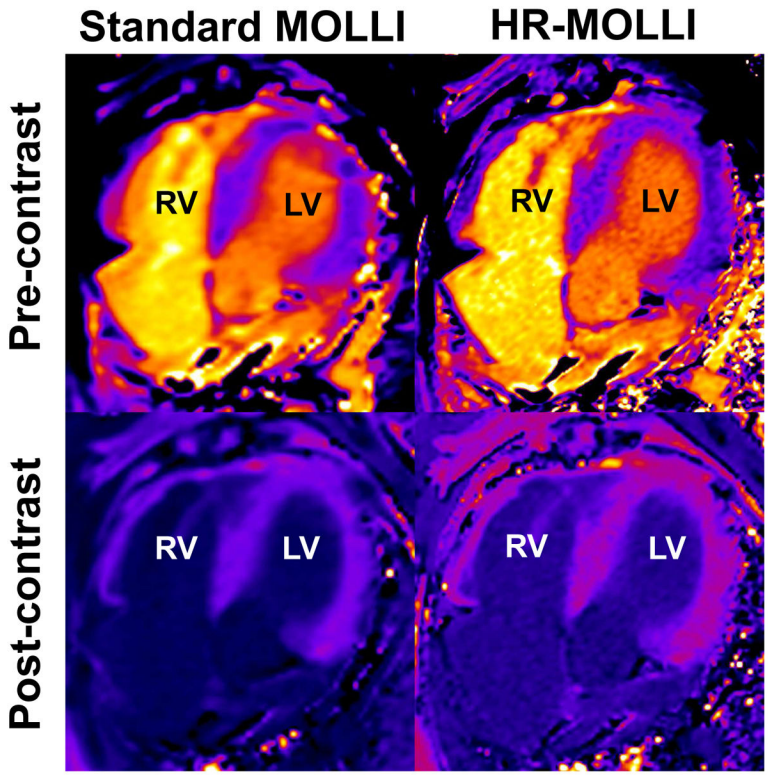

Figure 3. Right ventricular T1 mapping on cardiac magnetic resonance imaging

As compared to standard MOLLI, the high-resolution (HR) MOLLI images (right panel) have a higher pixel density and therefore may be more accurate for estimating extracellular volume content in the thin-walled right ventricular myocardium.

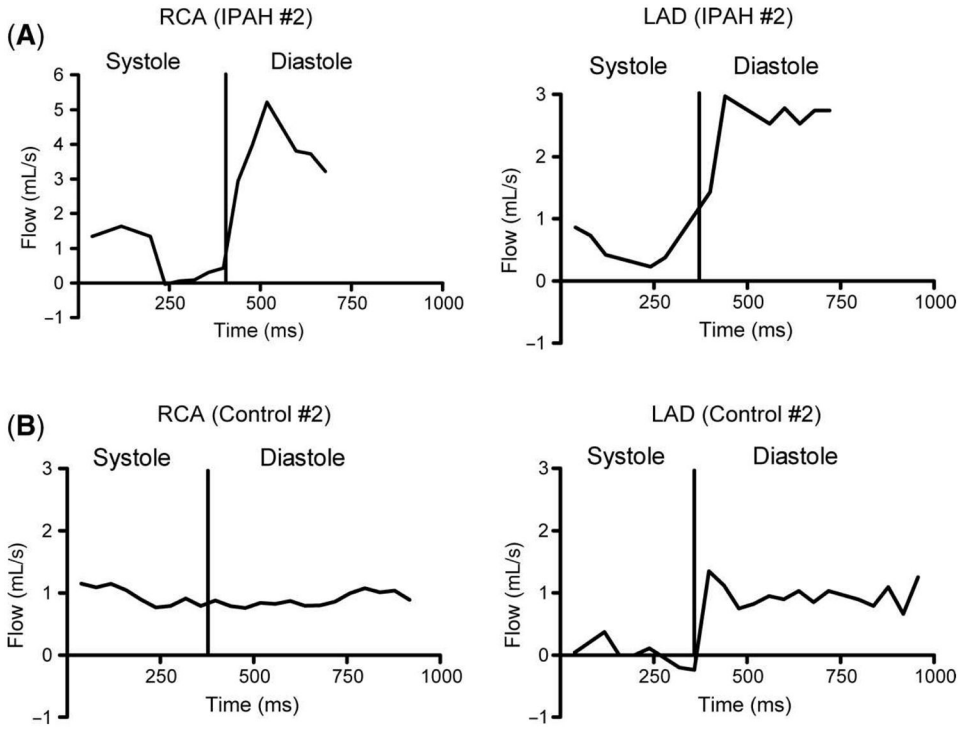

Figure 4. Representative examples of the right coronary artery and left anterior descending flow curves, obtained on cardiac magnetic resonance imaging

Top panel: idiopathic pulmonary arterial hypertension; bottom panel: healthy control (below). Systolic and diastolic phase in the cardiac cycle are indicated. Reproduced with permission from van Wolferen SA, et al. *Eur Heart J* 2008; 29:120–127.

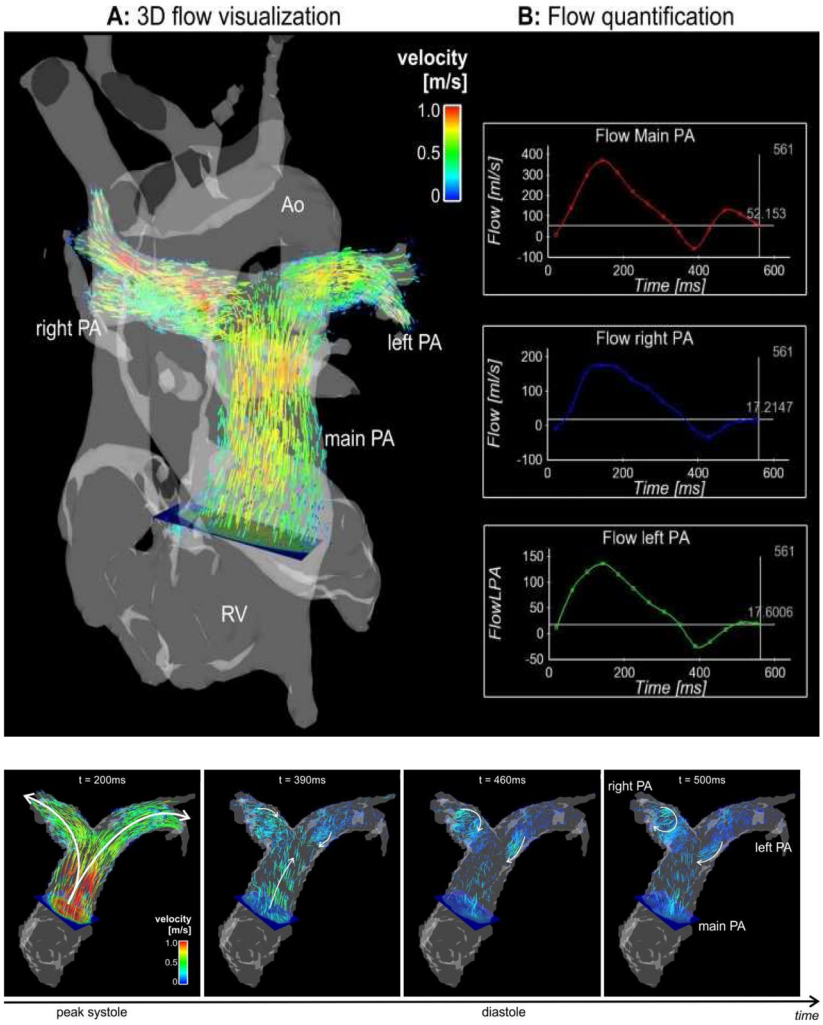

Figure 5. 4D flow magnetic resonance imaging

Top panel: whole heart 4D flow MRI in a healthy control subject and 3D visualization of peak systolic pulmonary flow (A). Retrospective placement of analysis planes in the main pulmonary artery (PA) and branches can be used for flow quantification (B). Ao: aorta, RV: right ventricle. Bottom panel: 4D flow MRI in a patient with pulmonary arterial hypertension. 3D visualization of pulmonary blood flow over the cardiac cycle illustrates peak systolic out flow and diastolic retrograde flow patterns and vortex formation in both the left and right pulmonary arteries (PA).

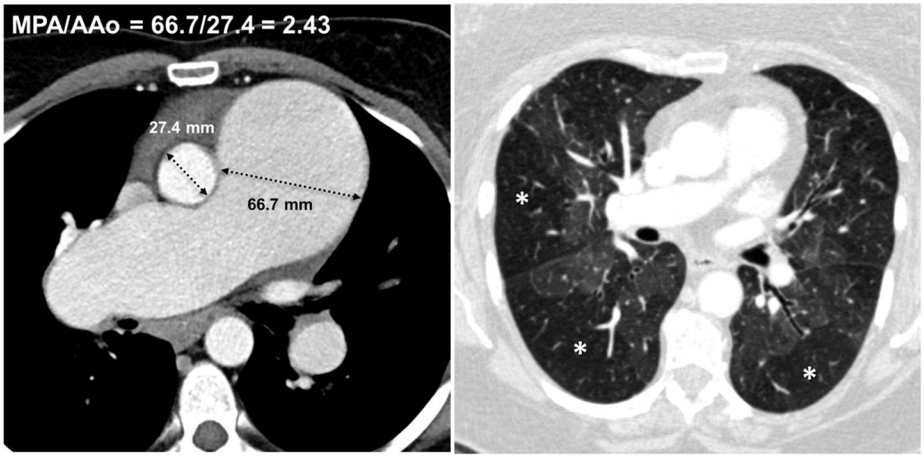

Figure 6. Examples of the role of computed tomography imaging in pulmonary hypertension

Left panel: CT angiography images from a 43-year-old female with idiopathic PAH demonstrating severe enlargement of the main pulmonary artery and increased ratio of the main pulmonary artery to ascending aorta diameter (2.4). MPA = main pulmonary artery; AAo = ascending aorta. Right panel: 65-year-old female with chronic thromboembolic pulmonary hypertension. CT chest reveals “mosaic” lung attenuation due to heterogeneous lung perfusion with darker areas (*) indicating hypoperfusion.

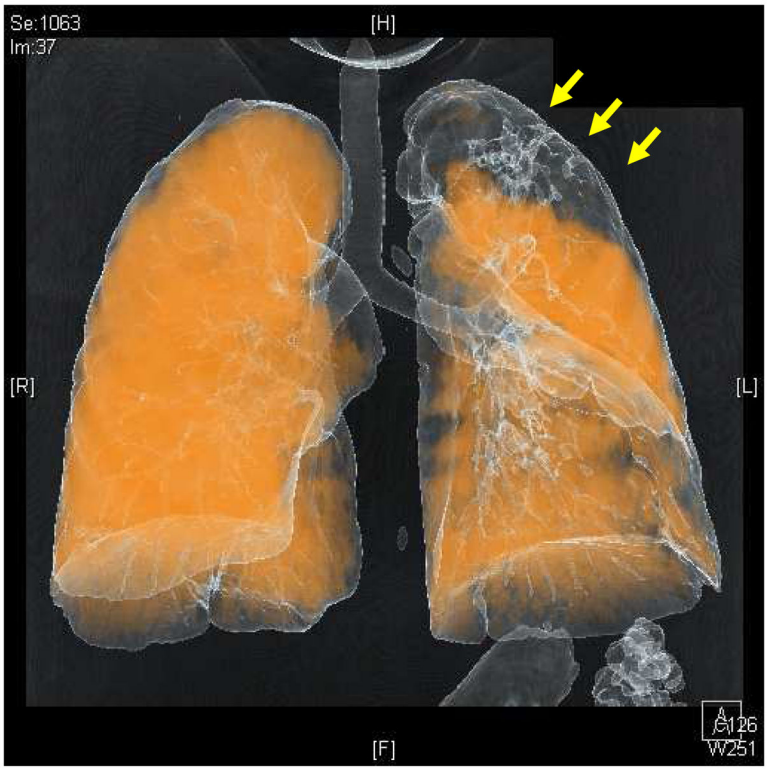

Figure 7. Example of dual source computed tomography demonstrating lung perfusion abnormalities in a patient with chronic thromboembolic pulmonary hypertension

The left upper lung hypoperfusion (arrows) corresponded with the area of largest thrombus burden in the patient.

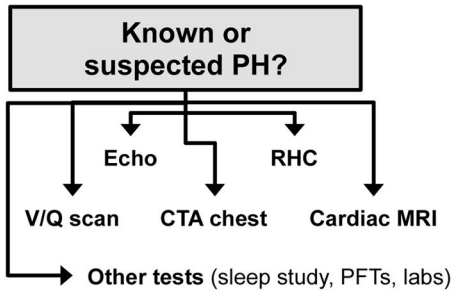

Echocardiographic differentiation: PAH vs. PVH

Parameter	PAH	PVH
RV size	Enlarged	May be enlarged
LA size	Small	Large
RA/LA size ratio	Increased	Normal (LA > RA size)
Interatrial septum	Bows from right to left	Bows from left to right
RVOT notching	Common	Rare
E/A ratio	<< 1	> 1
Lateral e' velocity	Normal	Decreased
Lateral E/e'	< 8	> 10

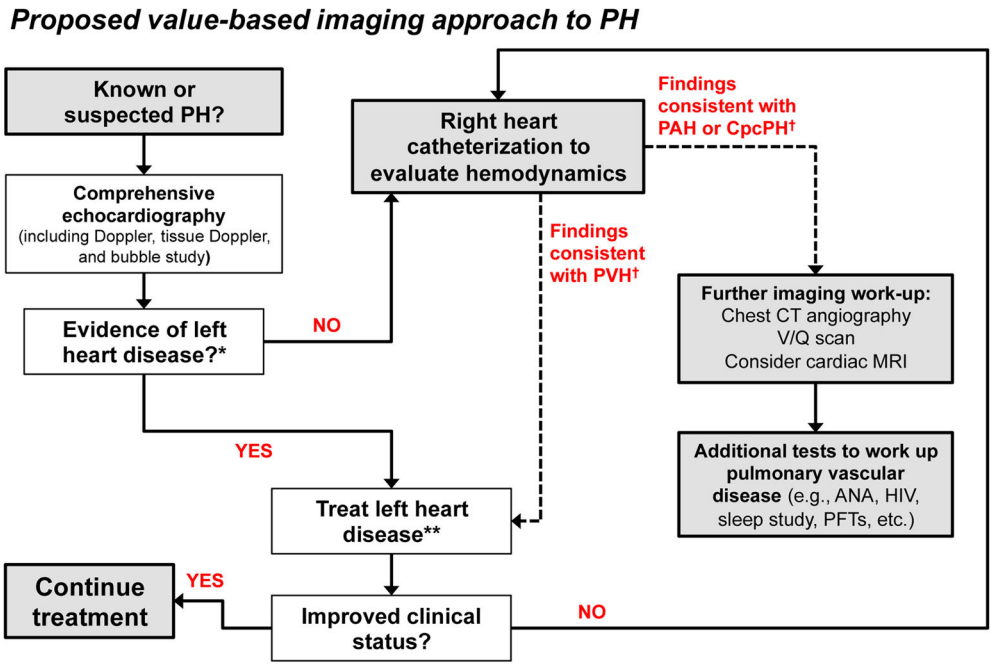

Figure 8. Proposed algorithm to enhance value-based imaging in patients with suspected or known pulmonary hypertension

PH = pulmonary hypertension; CTA = computed tomography angiography; RHC = right heart catheterization; V/Q = ventilation/perfusion; MRI = magnetic resonance imaging; RV = right ventricle; RA = right atrium; LA = left atrium; RVOT = right ventricular outflow tract; ANA = anti-nuclear antibody; HIV = human immunodeficiency virus; PFT = pulmonary function test; PAH = pulmonary arterial hypertension; PVH = pulmonary venous hypertension; CpcPH = combined post- and pre-capillary pulmonary hypertension.

Top left panel: current "shotgun approach" to imaging and other tests in the work-up of pulmonary hypertension. Bottom panel: proposed value-based imaging algorithm for work-up of PH. Since most patients with PH have left heart disease, the echocardiogram is the focus of initial work-up and if findings are consistent with pulmonary venous hypertension, treatment for left heart disease is recommended first before automatically proceeding to other tests (including invasive hemodynamic testing). Top right panel: helpful

echocardiographic clues for the differentiation between pulmonary arterial hypertension and pulmonary venous hypertension.

*See right upper panel for echocardiographic clues of left heart disease; other signs of left heart disease include reduced left ventricular ejection fraction, aortic valve disease, and mitral valve disease.

**Treatment of left heart disease is dependent on the underlying etiology of left heart disease; however, pulmonary hypertension in most patients with left heart disease will improve with diuresis and lowering systemic blood pressure (i.e., systemic vasodilation).

†PAH is characterized by mean pulmonary artery pressure ≥ 25 mmHg and pulmonary capillary wedige pressure ≤ 15 mmHg; pulmonary venous hypertension is characterized by mean pulmonary artery pressure ≥ 25 mmHg and pulmonary capillary wedge pressure > 15 mmHg; combined post- and pre-capillary pulmonary hypertension is characterized by pulmonary venous hypertension *plus* diastolic pulmonary gradient (PADP-PCWP) > 7 mmHg or pulmonary vascular resistance > 3 Wood units.

Table 1

Diagnostic Criteria and Categorization of Pulmonary Hypertension

		All WHO Groups	WHO Group 1	WHO Group 2	WHO Group 3	WHO Group 4	WHO Group 5
Description		Elevated pulmonary artery pressure	Pulmonary arterial hypertension	Pulmonary venous hypertension	PH due to hypoxemia	Chronic thromboembolic PH	Miscellaneous or multifactorial PH
Major etiologies			Idiopathic, heritable, drug/toxin-induced, HIV, CTD, portal hypertension, CHD (shunts), schistosomiasis (WHO Group 1' includes PVOD and PCH)	LV systolic dysfunction, LV diastolic dysfunction, aortic valve disease, mitral valve disease	COPD, interstitial lung diseases, sleep-disordered breathing		Chronic hemolytic anemias, myeloproliferative disorders, sarcoidosis, glycogen storage disease, thyroid diseases, chronic kidney disease
Estimated prevalence		Up to 10–20% of the general population	15 cases per million overall, 6 cases per million for idiopathic PAH	> 3–4 million in the United States	20% in COPD patients with a prior hospitalization for COPD exacerbation, >50% in advanced COPD; 32–39% in interstitial lung disease	0.5–2% (up to 3.8%) in survivors of acute pulmonary embolism	Unclear
Diagnostic criteria	Mean PA pressure (mmHg)	≥ 25	≥ 25	≥ 25	≥ 25	≥ 25	≥ 25
	PCWP or LVEDP (mmHg)	—	≤ 15	> 15	≤ 15	≤ 15	≤ 15
	PVR (dynes/s/cm^5)	—	> 240	—	> 240	> 240	> 240

Abbreviations: WHO, World Health Organization; PH, pulmonary hypertension; HIV, human immunodeficiency virus; PA, pulmonary artery; PCWP, pulmonary capillary wedge pressure; LVEDP, left ventricular end-diastolic pressure; PVR, pulmonary vascular resistance; COPD, chronic obstructive pulmonary disease; HIV, human immunodeficiency virus; CTD, connective tissue diseases; CHD, congenital heart diseases; LV, left ventricular; PVOD = pulmonary veno-occlusive disease; PCH = pulmonary capillary hemangiomatosis

Table 2

Key Parameters on Magnetic Resonance Imaging in the Evaluation of Patients with Pulmonary Hypertension

MRI Parameter	MRI Sequence Details	Key points
RV size and function	• bSSFP ECG-gated cine • Short axis or transaxial plane	• Reference standard • Delineation of tricuspid valve plane challenging on short axis imaging • Superior reproducibility makes it ideal for clinical trials • SV, RVEF, RV volumes are all prognostic variables in PH
Interventricular septal changes	• bSSFP ECG-gated or real- time cine imaging • Short-axis plane	• Provides insight into degree of RV pressure and volume overload • Septal shift during cardiac cycle prognostic marker in PH
PA pulsatility (relative area change)	• 2D PC-MRI • GRE or bSSFP ECG-gated cine	• PA pulsatility prognostic marker in PH
PA mean transit time	• TR-MRA	• Significant prognostic marker in PH • MRA is also helpful in differentiating between COPD, interstitial lung disease, and chronic thromboembolic disease
RVIP delayed enhancement RV diffuse interstitial abnormalities	• LGE • RV T1 mapping	• RVIP associated with worse outcomes in PH • RV interstitial abnormalities potentially identify diffuse fibrosis within the RV
RV strain	• Myocardial tagging • HARP • DENSE • SENC • Feature tracking • Deformation field analysis	• Provides RV longitudinal, circumferential, and radial strain measurements • Changes in regional strain potentially useful in understanding mechanism of disease
RV perfusion	• First pass perfusion • Vasodilator needed for stress perfusion	• Detects changes in RV coronary flow • Significant difference in these markers between PH patients and controls
PA peak velocity PA average flow PA time-to-peak velocity PA velocity-rise gradient PA and RV vortex flow	• 2D PC-MRI • 4D flow MRI	• Significant differences in these markers between PH patients and controls • Altered flow patterns recognized in the PA of PH patients

MRI Parameter	MRI Sequence Details	Key points
PA wall shear stress		• Wall shear stress lower in PH patients compared to controls

Table 3

Indices of Pulmonary Artery Stiffness Derived from Cardiac Magnetic Resonance Imaging and Invasive Hemodynamic Testing

Parameter	Units	Formula	Definition
Pulsatility (also known as relative area change [RAC])	%	(maxA-minA)/minA × 100 *or* (maxA-minA)/maxA × 100 *	Relative change in lumen area during the cardiac cycle
Compliance	mm^2/mm Hg	(maxA-minA)/PP	Absolute change in lumen area for a given change in pressure
Capacitance	mm^3/mm Hg	SV/PP	Change in volume associated with a given change in pressure
Distensibility	%/mm Hg	(maxA-minA)/PP × minA × 100	Relative change in lumen area for a given change in pressure
Elastic modulus	mm Hg	PP × minA/(maxA-minA)	Pressure change driving a relative increase in lumen area
Stiffness index β	N/A	*Ln*(PASP/PADP)/((maxA-minA)/minA)	Slope of the function between distending arterial pressure and arterial dimension

* Pulsatility (RAC) is variably defined in the literature.

PASP = pulmonary artery systolic pressure; PADP = pulmonary artery diastolic pressure; maxA = maximum area of the proximal pulmonary artery; minA = minimum area of the proximal pulmonary artery; SV = stroke volume; PP = pulse pressure Modified with permission from Sanz et al. JACC Cardiovasc Imaging 2009; 2:286–95

Table 4

Computed Tomography Findings That Are Useful For the Evaluation of Pulmonary Hypertension and its Etiologies

Clinical entity	Non-contrast CT findings and caveats
Pulmonary hypertension	• Findings suggestive of PH: dilated PA, increased main PA:AAo ratio, PA calcification, tortuosity of the PAs, rapid tapering of the PAs, and mosaic attenuation of the lung parenchyma. • Cut-offs for main PA diameter and main PA:AAo ratio are based on data from the Framingham Heart Study. 90th percentile cutoff values were >29 mm main PA diameter in men, >27 mm main PA diameter in women, and 0.9 main PA:AAo ratio. • Additional findings of PH on CT angiography include reflux of intravenous contrast into the hepatic veins, RV dilation, RV hypertrophy, flattening or bowing of the interventricular septum, and dilation of the bronchial arteries.
Etiologies of pulmonary hypertension	
• COPD	• In patients with COPD, CT can confirm the presence and characterize the type of emphysema, airway disease and secondary features associated with COPD. • Quantitative methods of assessing emphysema severity have been developed and correlate with histological and clinical indices of COPD severity. • Main PA diameter and main PA:AAo ratio in COPD are linearly correlated with systolic, diastolic and mean PA pressures.
• HHT	• On non-contrast CT, pulmonary arteriovenous malformations present as a nodular opacity with a feeding artery and a draining vein. • Contrast-enhanced CT angiography is only necessary for the evaluation of larger pulmonary arteriovenous malformations or in patients that have already undergone embolization.
• ILD	• Non-contrast high-resolution CT is the test of choice for the parenchymal evaluation of ILD. • Caution must be used when measuring main PA diameter in patients with pulmonary fibrosis, because main PA dilation can occur in the absence of PH in these patients.
• PVOD	• CT features that are suggestive of PVOD include smooth septal lines, centrilobular ground glass opacities and enlarged lymph nodes.
• CTEPH	• CT metrics, including main PA diameter, RV/LV diameter ratio, and RV wall thickness correlate with mean PA pressure in CTEPH.

PA = pulmonary artery; AAo = ascending aorta; CT = computed tomography; RV = right ventricular; COPD = chronic obstructive pulmonary disease; HHT = hereditary hemorrhagic telangiectasia; ILD = interstitial lung disease; PVOD = pulmonary veno-occlusive disease; CTEPH = chronic thromboembolic pulmonary hypertension; LV = left ventricular

Table 5

Relative Costs for Imaging Tests Used in the Diagnosis and Management of Pulmonary Hypertension (Centers for Medicare and Medicaid Services Data*)

CPT code	Procedure	Technical fee (US dollars)	Professional fee (US dollars)	Global fee (US dollars)
71275	CT angiography chest	228.09	102.07	330.15
75561	Cardiac MRI with contrast	307.00	131.52	427.61
93306	Transthoracic echocardiography with Doppler	165.65	64.32	229.97
93312	Transesophageal echocardiography with Doppler	186.14	123.61	309.75
78585	V/Q scan	295.37	53.90	349.27
93451	Right heart catheterization	647.88	150.20	798.08

CT = computed tomography; MRI = magnetic resonance imaging; V/Q = ventilation/perfusion

*Data obtained from https://www.cms.gov/apps/physician-fee-schedule/overview.aspx

Table 6

Completed Pulmonary Hypertension Clinical Trials with Cardiac Magnetic Resonance Imaging-Based Endpoints

Study (year)	Type of study	# of patients	Intervention	Study duration	CMR endpoints	Summary of results
Wilkins SERAPH (2005)	RCT	26 PAH	Sildenafil vs Bosentan	4 months	RV mass	RV mass decreased with both sildenafil and bosentan (mean 8.8 g vs. 3 g; p=0.142)
Wilkins SiPHT (2010)	RCT	42 PAH	Simvastatin add-on	12 months	RV mass	Simvastatin produces a 5.2 g mean decrease in RV mass within 24 weeks that is not sustained at 12 months
Roeleveld (2004)	Prospective observational study	11 PAH	Epoprostenol	12 months	RV mass RVEDV	No significant change in RV mass or RVEDV
Van Wolferen (2006)	Prospective observational study	15 PAH	Bosentan with Sildenafil add-on	3 months	RV mass RVEF RVEDV	On average, sildenafil add- on decreased RV mass by 8 g (p<0.01) and increased RVEF by 4% (p<0.05), No significant change in RVEDV
Chin (2008)	Prospective observational study	16 PAH	Bosentan	12 months	RVEF RVEDV SV	No significant change in RVEF, RVEDV, or SV
Euro MR (2010)	Prospective observational study	91 PH	None (physician-discretion therapy)	12 months	RVEDVI RVSVI RVEF RV mass index	Significant improvement in RVEF (p<0.001) and RVSVI (p<0.0001)

SERAPH = Sildenafil versus Endothelin Receptor Antagonist for Pulmonary Hypertension

SiPHT = Simvastatin Pulmonary Hypertension Trial

RCT = randomized controlled trial

PAH = pulmonary arterial hypertension

RV = right ventricular

RVEDV(I) = right ventricular end-diastolic volume (index)

RVEF = right ventricular ejection fraction

SV(I) = stroke volume (index)